International Journal of Science and Research (IJSR)
ISSN (Online): 2319-7064
Impact Factor (2012): 3.358

Growth, Optical, Mechanical and Dielectric Properties of Potassium Tetraborate Tetrahydrate Single Crystal

S. Sathiskumar[1], T. Balakrishnan[2], K. Ramamurthi[3]

[1,2,3] Crystal Growth Laboratory, PG & Research Department of Physics, Periyar EVR College (Autonomous),
Tiruchirappalli – 620 023, Tamil Nadu, India

Abstract: ***Potassium tetraborate tetrahydrate (KTBTH) single crystals were grown by slow evaporation solution growth method at room temperature. The grown crystal was characterized by single crystal X - ray diffraction analysis. FT – IR and FT – Raman spectra were recorded to identify the functional groups. Optical transmission and absorption spectral studies were carried out to test the transmittance of the crystal in the UV – visible – NIR range. Optical parameters such as band gap energy and extinction coefficient of the grown crystal were calculated. Mechanical hardness of the grown crystal was estimated by Vickers microhardness test. Dielectric constant and dielectric loss of KTBTH crystal were calculated as a function of frequency at different temperatures. The a.c. resistivity and a.c. conductivity were obtained from the dielectric studies. Etching studies were carried out for different etching time. Kurtz powder second harmonic generation (SHG) test reveals that KTBTH possesses SHG efficiency of 0.4 times that of urea, thus shows it a potential candidate for optical second harmonic generation.***

Keywords: Crystal growth, Optical properties, Mechanical properties, Dielectric constant

1. Introduction

Nonlinear optical (NLO) materials find applications in potential areas like optical modulation, optical switching, optical logic and optical memory, telecommunication, signal processing and optical internal connections [1]. In this regard inorganic borates have long been in the focus of researchers due to their interesting variety of structures, high laser damage threshold and high optical quality. The boron atom usually coordinates with either three / four oxygen (or) fluorine atoms to form $[BO_3]^{3-}$ or $[BO_4]^{5-}$ or $[BF_4]^{-}$ groups [2]. Accordingly, the electronic orbitals of the boron atoms are hybridized to forming sp^2 structures with trigonal symmetry or sp^3 structures exhibiting tetragonal symmetry. Moreover several of these two kinds of groups can be connected in different ways to form typical B_xO_y structures [3]. Thus the ability of boron atoms to form various structural possibilities makes the borates an attractive candidate in the field of nonlinear optics. Crystals containing the basic $[BO_3]^{3-}$ and $[BO_4]^{5-}$ groups are noncentrosymmetric [4]. Due to such special features of the borate groups, the search on the noncentrosymmetric crystal structures in borate family and the novel materials reported is about twice when compared to the families of other crystals [5]. In addition, borate crystals have the advantages of low absorption edge with high transmittance region and possessing high laser damage threshold and reasonable NLO coefficient. Extensive search has led to the discovery of many excellent materials such as β - BaB_2O_4 [6], LiB_3O_5 [7], ammonium pentaborate [8], potassium pentaborate [9], potassium boromalate [10], potassium boro succinate [11], rubidium bis – DL malatoborate [12] and strontium teribium triborate [13]. The single crystal structure of potassium tetraborate tetrahydrate (KTBTH) ($K_2[B_4O_5(OH)_4].2H_2O$) was reported by Marezio et al. [14] and KTBTH belongs to orthorhombic crystal structure with the space group of $P2_12_12_1$, a noncentrosymmetric structure. Growth of KTBTH crystal and its thermal and linear optical properties of KTBTH were reported by Hellwig et al. [15] and Xingcheng Luo et al. [16]. In the present work studies on the growth, spectroscopic, linear and nonlinear optical, dielectric, etching and powder second harmonic generation efficiency of KTBTH crystal are carried out and presented.

2. Experimental

2.1. Crystal Growth

Potassium hydroxide (KOH) and boric acid (H_3BO_3) were dissolved in double distilled water at room temperature. Then the resultant solution was stirred well to obtain clear solution. The solution was filtered using Whatman filter paper and taken in a beaker. Beaker containing the solution was closed with polythene sheet containing small pinholes and it was kept in a dust free atmosphere. Solvent evaporation at room temperature yielded transparent single crystals of KTBTH of 5 mm × 4 mm × 3 mm size in a growth period of 10 days (Fig.1).

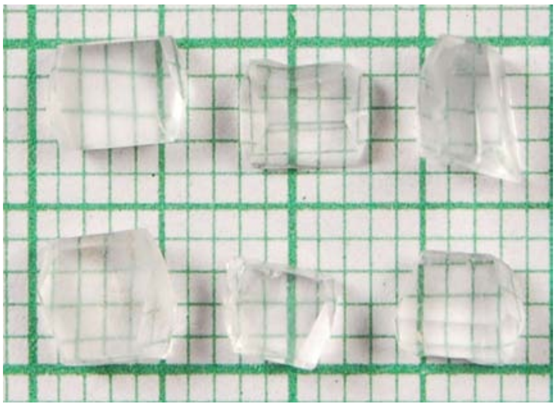

Figure 1: As grown KTBTH crystals

3. Characterization Studies

3.1 X – ray Diffraction Analysis

Single crystal X – ray diffraction intensity data were collected on a BRUKER NONIUS CAD4 single crystal X - ray diffractometer using monochromatized Cu Kα radiation (λ = 1.5408Ǻ) at 293K. The results show that the KTBTH belongs to orthorhombic system with unit cell parameters a = 6.855 (6.859) Ǻ, b = 11.778 (11.774) Ǻ, c = 12.894 (12.899) Ǻ and they compare well with the corresponding reported values of Hellwig et al. [15] given in the parenthesis.

3.2 FT – IR and FT – Raman Spectral Analyses

Fourier transform infrared (FT - IR) spectral analysis of KTBTH single crystal was carried out between 4000 and 400 cm^{-1} using Perkin Elmer FT – IR spectrophotometer by KBr pellet technique at 300 K. FT – IR spectrum of KTBTH is shown in Fig. 2. The O – H asymmetric and symmetric stretching vibrational frequencies are observed at 3562 and 3378 cm^{-1} respectively. The peak at 1690 cm^{-1} is due to O – H bending vibration. The band observed at 1096 and 1000 cm^{-1} are due to B – O terminal asymmetric and terminal symmetric stretching vibrations respectively. The intense sharp peak observed at 1243 cm^{-1} is assigned to O - B - O asymmetric stretching vibration. Strong band observed at 831 cm^{-1} is due to B – O stretching vibration. The O - B - O ring asymmetric bending vibration is observed at 712 cm^{-1}. The peak observed at 449 cm^{-1} is attributed to B – O stretching vibration [17, 18]. FT – IR and FT – Raman vibrational frequencies and their assignments are compared in Table 1.

Fourier Transform – Raman spectrum of KTBTH was recorded using Bruker RFS 27 spectrophotometer and is shown in Fig.3. The B – O terminal asymmetric stretching vibration is observed at 1092 cm^{-1} and the O - B - O bending vibration is observed at 568 cm^{-1}. The B – O stretching vibration appears at 455 cm^{-1} with strong intensity [17, 18].

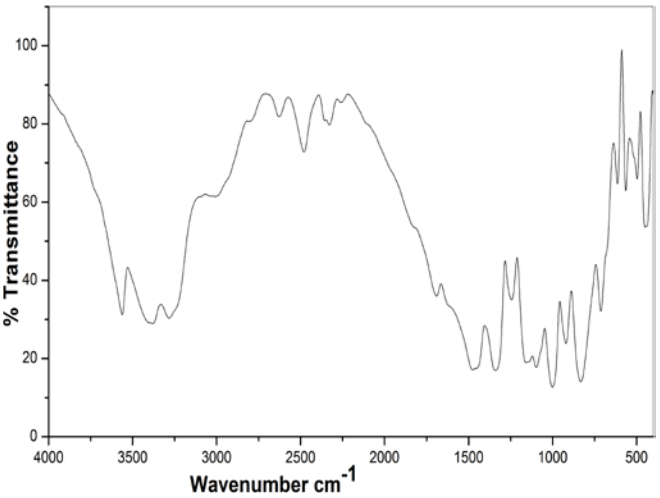

Figure 2: FT – IR spectrum of KTBTH

Table 1: Comparison of FT – IR and FT – Raman spectral frequencies (cm^{-1}) of KTBTH crystal

FT – IR	*FT – Raman*	*Band assignments*
3562	-	O – H asymmetric stretching
3378	-	O – H symmetric stretching
1690	-	O – H bending
1475	1410	B – O terminal asymmetric stretching
1339	-	B – O asymmetric stretching
1243	-	O – B – O asymmetric stretching
1158	-	B – O terminal stretching
1096	1092	B – O terminal asymmetric stretching
1000	974	B – O terminal symmetric stretching
920	-	B – O ring stretching
831	-	B – O stretching
-	765	B – O ring stretching
712	695	O – B – O ring asymmetric bending
613	591	O – B – O terminal bending
564	568	O – B – O bending
496	-	O – B – O stretching
449	455	B – O stretching

3.3 UV – Vis – NIR Spectral Studies

UV – Vis - NIR optical transmission spectrum was recorded in the range of 190 – 1100 nm using THERMO SCIENTIFIC spectrophotometer. The transmittance and absorbance spectrum of KTBTH single crystal of thickness~ 3mm is presented in Fig. 4. The crystal possesses high transmittance of 95 %, the essential properties of any crystal for NLO applications. The π – π* orbital transition occurs in the excitation of π electron requires smaller energy and hence, transition of this type occurs at longer wavelength. Lower cut off wavelength occurs at 200 nm and there is no absorption in the entire visible region. The optical absorption coefficient (α) is calculated using the relation [19],

$$\alpha = \frac{1}{t}\log\left(\frac{1}{T}\right) \qquad (1)$$

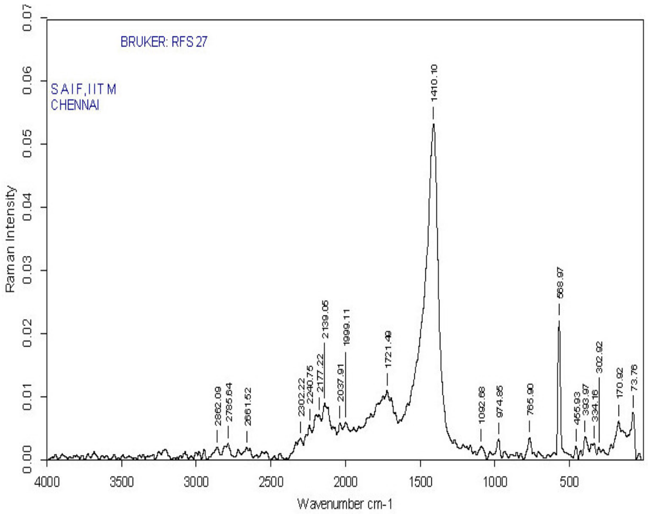

Figure 3: FT – Raman spectrum of KTBTH

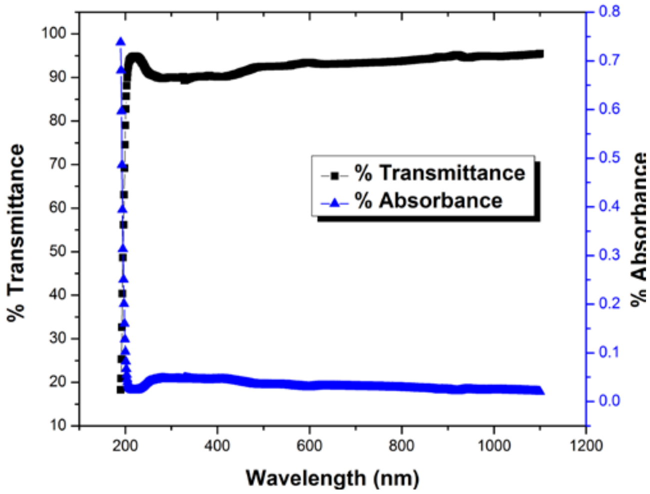

Figure 4: UV – Vis – NIR transmittance and absorbance spectrum of KTBTH

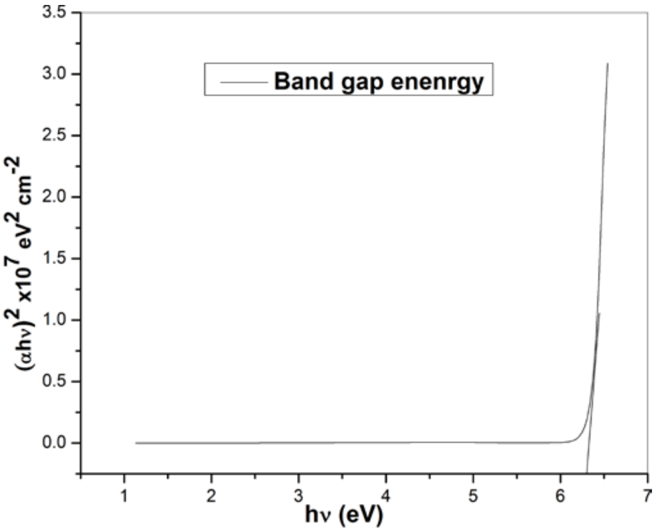

Figure 5: Plot of $(\alpha h\upsilon)^2$ versus photon energy for KTBTH

where T is the transmittance and t is the thickness of the crystal. The direct band gap of the crystal can be obtained from the absorption coefficient (α) calculated using the relation [20],

$$\alpha = \frac{A(h\upsilon - Eg)^{1/2}}{h\upsilon} \qquad (2)$$

where E_g is the optical band gap energy of the crystal, h is the Planck's constant, υ is the frequency and A is a constant. A plot of variation of $(\alpha h\upsilon)^2$ versus hυ is shown in Fig. 5. E_g is evaluated by extrapolating the linear portion of the graph. The direct energy gap is ~ 6.3 eV. The high value of band gap shows the crystal possesses dielectric behavior to induce polarization when powerful radiation is incident on the material. The absorption coefficient (α) is related to the extinction coefficient K by the relation [21]

$$K = \frac{\alpha\lambda}{4\pi} \qquad (3)$$

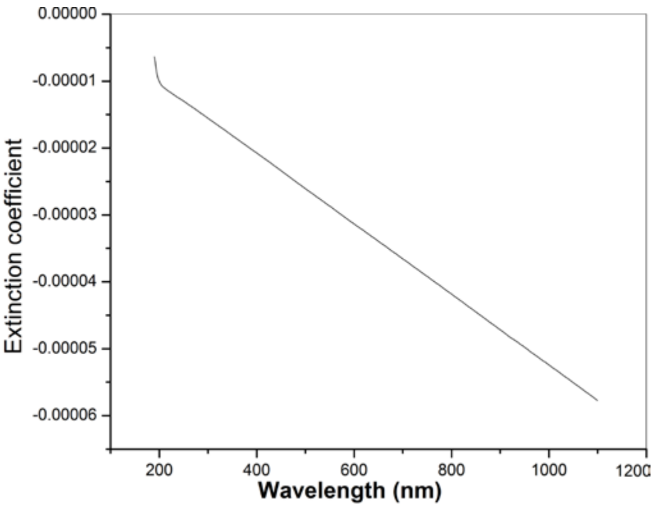

Figure 6: Plot of extinction coefficient (K) vs. wavelength

where λ is the wavelength and α is the absorption coefficient. Fig. 6 shows the variation of extinction coefficient as a function of wavelength. The optical parameter of transmittance and extinction coefficient of the grown crystal shows that KTBTH can be used as a potential material for NLO applications.

3.4 Microhardness Studies

The structure and molecular composition of crystals greatly influence their mechanical properties. Microhardness test is one of the simplest and best methods to understand the strength of the materials. Hardness of a material is a measure of resistance offered by the lattice for permanent deformation [22]. Shimadzu Vickers diamond pyramidal indenter was used for the microhardness studies. Microhardness measurements were made on the polished (100) plane of the KTBTH crystal. Load P was varied between 2 and 50g, and the time of indentation was kept constant (5s) for all trials. The diagonal lengths of indentation d_1 and d_2 were measured in µm for various applied load (P). The Vickers hardness number (Hv) was calculated using the relation [23]

$$H_v = \frac{1.8544P}{d^2} kg/mm^2 \qquad (4)$$

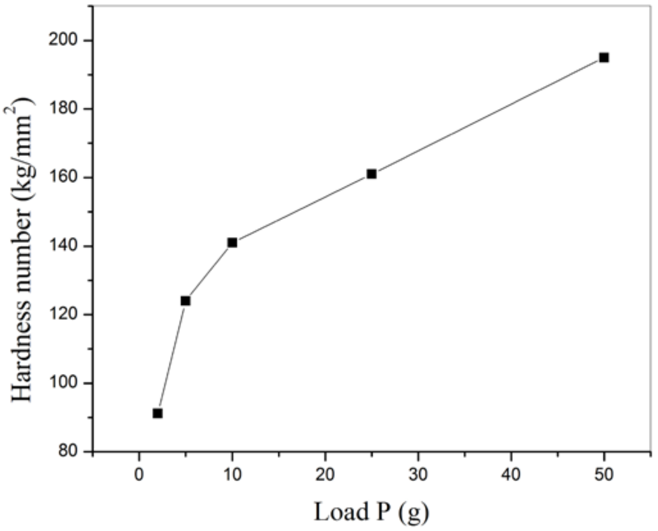

Figure 7: Microhardness values versus load for KTBTH

where *d* is the average value of d_1 and d_2. The variation of *Hv* with the applied load P is shown in Fig. 7. It is observed that the microhardness value increases with the increase in the applied load. According to the normal indentation size effect (ISE), microhardness of crystals decreases with increasing load and for reverse indentation size effect (RISE) hardness increases with increasing load [24]. In the present work the plot obtained between log P and log d gives a straight line. The work hardening coefficient (n) was calculated from Fig.8 by the least square curve fitting method. The work hardening coefficient (n) calculated is 3. Onitsch [25] concluded that if the value of n lies between 1 and 1.6 it refers to the hard materials and for soft materials it is above 1.6. Thus the KTBTH single crystal comes under the soft materials category. KTBTH exhibits the cracks for load (P) above 100g due to the release of internal stress generated locally by indentation. According to Meyer's law,

$$P = Ad^n \tag{5}$$

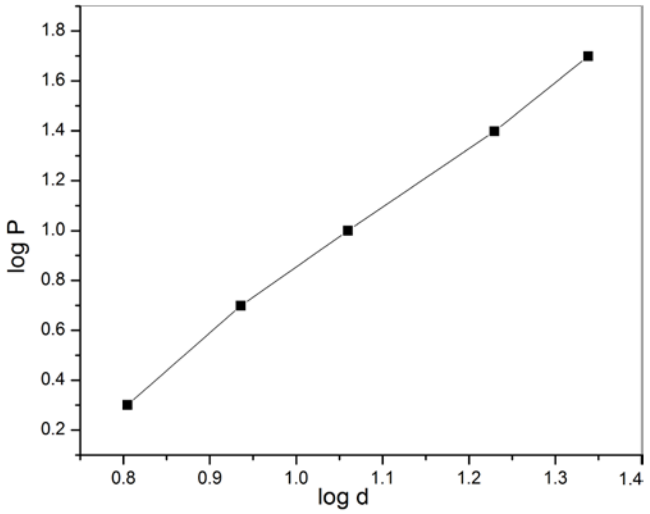

Figure 8: log P versus log d for KTBTH

where n is the Meyer's index or work hardening exponent and A is a material constant. Li and Bradt [26] explained the indentation size effect on the basis of the proportional specimen resistance (PSR) model. According to the PSR model, microhardness can be described with two different parts, the first term represents the resistance of the test specimen to elastic deformation and friction at the indentation / specimen facet interface or ISE regime and the second term represents the indentation load – independent part. In the indentation test load P is related to the indentation size d [26] as follows

$$P = a_1 d + a_2 d^2 = a_1 d + (P_0 / d_0^{\,2}) d^2 \tag{6}$$

where a_1 is the contribution of proportional specimen resistance to the apparent microhardness and a_2 is related to the load independent microhardness. P_0 is the critical applied test load above which microhardness becomes load independent and d_0 is the corresponding diagonal length of the indentation.

$$(P/d) = a_1 + (P_0 / d_0^{\,2}) d \tag{7}$$

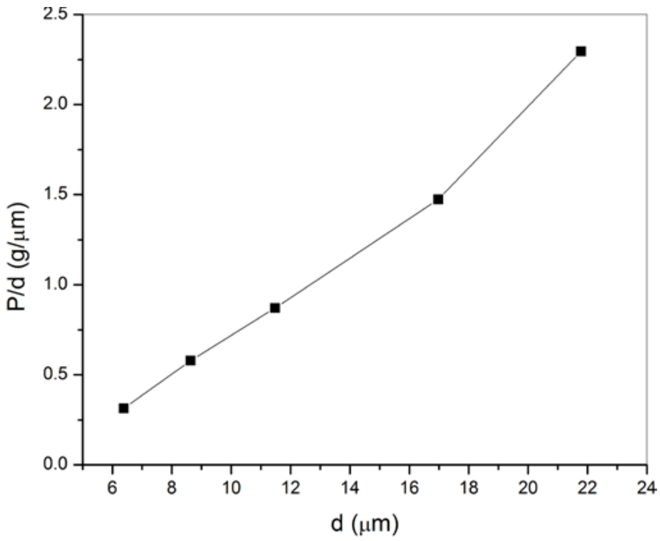

Figure 9: PSR plot of P/d versus d for KTBTH

A plot of (P/d) versus d gives a straight line Fig. 9, the slope of which gives the load independent microhardness. The slope (P/d^2) multiplied by the Vickers conversion factor (1.8544) gives the value of load independent microhardness. In the present study the calculated load independent microhardness is 100 g / mm^2.

3.5 Dielectric Studies

The dielectric study was carried out using the instrument HIOKI 3532 – 50 LCR HITESTER in the frequency range from 50 Hz to 2MHz at different temperatures. KTBTH single crystal of dimension 0.5 × 0.5 × 0.2 (cm^3) was taken and its opposite faces of the crystal were coated with silver paste. Then the crystal was placed between the two copper electrodes to form the parallel plate capacitor. The dielectric constant (ε) and dielectric loss (ε″) were calculated using equations

$$\varepsilon = \frac{Cd}{A\varepsilon_0} \tag{8}$$

$$\varepsilon'' = \varepsilon \tan\delta \tag{9}$$

where C is the capacitance of the sample, *d* is the thickness of the crystal, ε_0 is the permittivity of free space ($\varepsilon_0 \approx 8.854 \times 10^{-12}$ F / m) and *A* is the area of the sample. Experimental values of dielectric constant and dielectric loss of KTBTH crystal as a function of frequency is shown in Fig. 10 and Fig.11 respectively. From the figures it is observed that both the dielectric constant and dielectric loss decrease with increasing frequency. As the magnitude of dielectric constant depends on the degree of polarization of charge in the crystal and it arises from the contribution of different polarizations, namely electronic, ionic, orientation and space charge polarization [27, 28]. The large dielectric constant at low frequency is due to the presence of space charge polarization. Space charge polarization arises due to the mobile charge carriers impeded by interfaces. The space charge polarization depends on the bonding, structure, purity and perfection of the crystal [29]. The low value of dielectric constant at higher frequency is important for considering the materials for photonics, electro – optic and NLO applications. It is observed that the dielectric loss deceases with increasing frequency. The a.c. resistivity and a.c. conductivity are calculated using the relations [30].

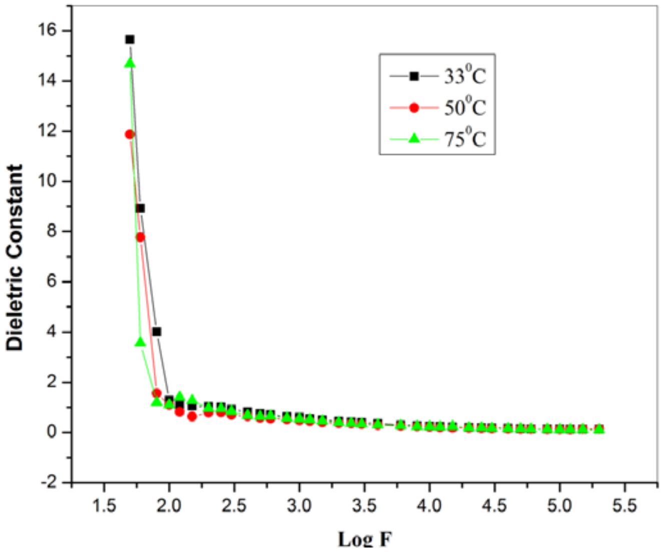

Figure 10: Variation of dielectric constant with log frequency

$$\rho = \frac{A}{2\pi fCd} \tag{10}$$

$$\sigma = \frac{1}{\rho} \tag{11}$$

The variation of a.c. resistivity and conductivity with the frequencies of applied field is shown in Fig.12 and Fig.13 respectively. As shown in Fig.12 the a.c. resistivity increases rapidly as frequency increases. Obviously the reverse trend is observed for a.c. conductivity (Fig. 13) of the grown crystal.

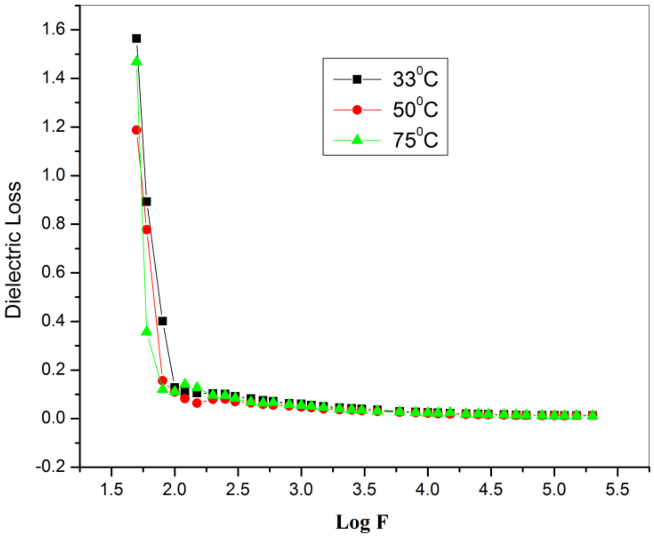

Figure 11: Variation of dielectric loss with log frequency.

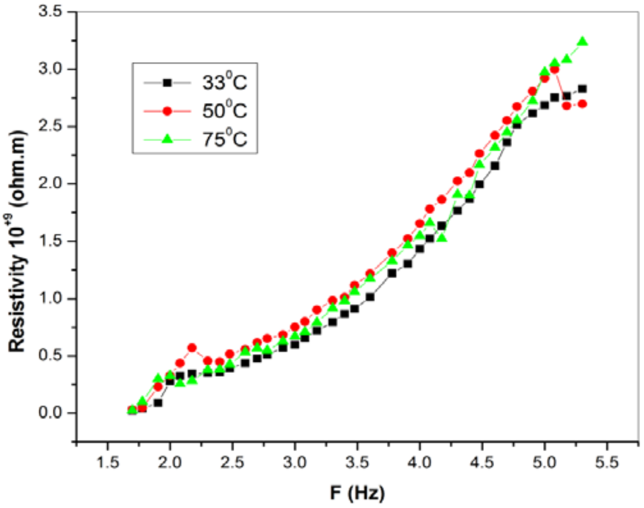

Figure 12: Variation in a.c. resistivity with the frequencies of grown crystal

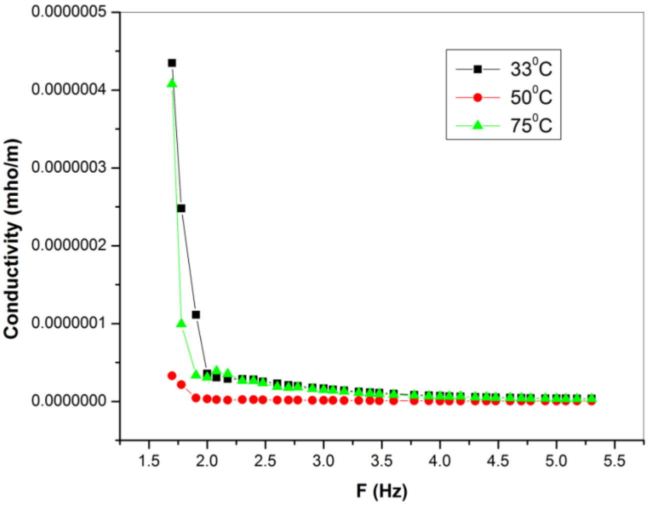

Figure 13: Variation in a.c. conductivity with the frequencies of grown crystal

3.6 Chemical Etching Studies

The chemical etching studies were carried out on the grown single crystal using polarized optical microscope fitted with Motic camera. Etching is an important tool for the identification of the crystal defects, which is able to develop some of the features such as growth hillocks, etch pits and grain boundaries on the crystal surface and micro structural imperfections of the grown crystal. Quality crystals with minimum defects for are essential fabrication of devices. Dislocations in crystal influence a number of physical properties like plasticity, mechanical strength, etc. [31]. Hence it is necessary to know the density and distribution of dislocations in the crystals. Chemical etching technique was employed for studying etch pit in the KTBTH crystal. Etching study was carried out on (110) plane of KTBTH crystal. KTBTH crystal was etched in diluted hydrochloric acid for duration of 5 and 10s. The etched samples were dried using tissue paper and etch pattern were observed. Fig. 14 shows the etch pattern on the (110) plane of grown KTBTH crystal for an etching time of 5s in diluted hydrochloric acid as etchant and it produces elongated rectangular hillock shaped well defined etch pits. Fig. 15 shows the etch pattern produced on the previously 5s etching face after an etching for additional 5s. An increase of etch time, does not make appreciable change in the morphology of the etch pits.

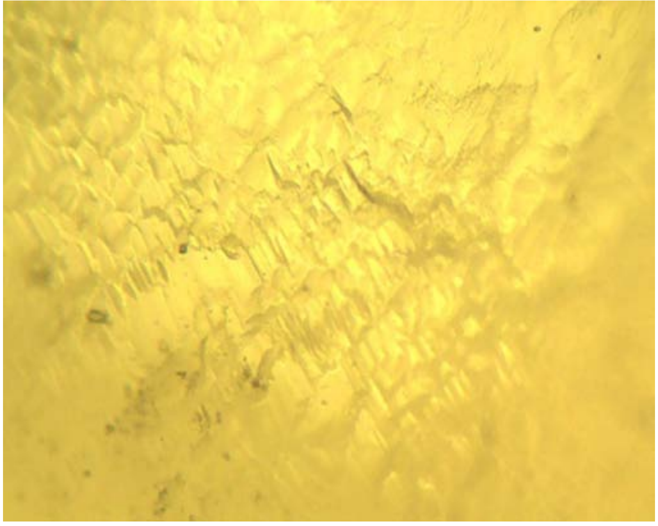

Figure 14: Etching study on (110) plane of KTBTH crystal (etch time of 5s)

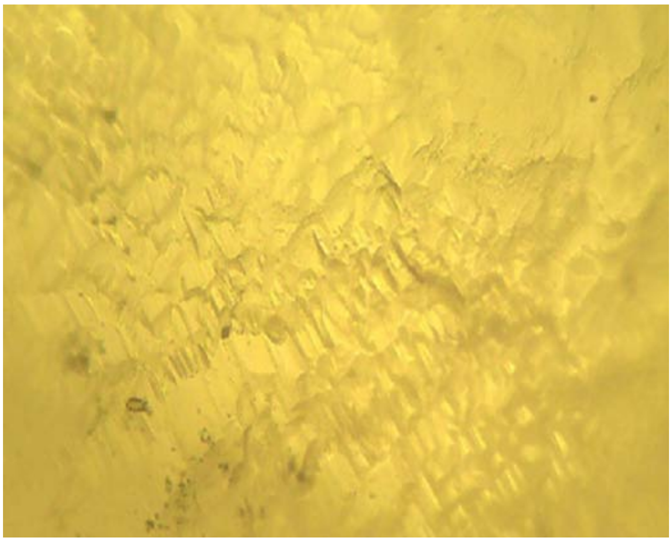

Figure 15: Etching study on (110) plane of KTBTH crystal (etch time of 10s)

3.7 Second Harmonic Generation

The second harmonic generation (SHG) efficiency test was carried out by the powder technique proposed by Kurtz and Perry [32]. A Q switched Nd:YAG laser beam of wavelength 1064 nm, with a beam energy of 0.680 J/pulse and a pulse with of 8ns with a repetition rate of 10Hz was used. The crystals are ground to powder and packed between two transparent glass slides and exposed to laser radiation. The second harmonic signal generated due to powdered crystal was confirmed from the emission of green radiation (532 nm). The observed SHG efficiency of KTBTH is~0.4 times that of urea crystal.

4. Conclusion

Optical quality single crystals of KTBTH were grown by slow evaporation solution growth technique using double distilled water. The single crystal XRD analysis reveals that the KTBTH belongs to orthorhombic system. Vibrational frequency of the functional groups present in the grown crystal was studied by FT – IR and FT – Raman analyses. The lower cut off wavelength is observed at 200 nm from UV – Vis – NIR transmittance spectrum. Extinction coefficient was calculated from the UV – Vis – NIR absorbance spectrum. Increase in the microhardness value with increase of load, brings out the reverse indentation size effect in KTBTH crystal. The load independent microhardness value for KTBTH is 40 g/mm^2. The dielectric studies revealed that the dielectric constant and dielectric loss decreases with increasing frequency at different temperatures. The a.c. resistivity of KTBTH increases with applied frequencies and a reverse effect is observed in a.c. conductivity. Etching study is made on (110) plane of the grown crystal with different two etching times and when the etching time is increased, there is no change in the morphology of the etch pits. The second harmonic generation efficiency of KTBTH is 0.4 times that of urea.

5. Acknowledgement

The authors T. B and S. S would like to acknowledge the University Grant Commission (UGC), New Delhi, India for providing financial support [project ref. No. 41 – 956/2012(SR)]. The scientific supports extended by Sophisticated Analytical Instrument Facility (SAIF), Indian Institute of Technology Madras, Chennai – 600 036, India, and Department of Physics, B. S. Abdur Rehman University, Vandalur, Chennai – 600 048, for providing facilities for characterization.

References

[1] Tanusri Pal, Tanusree Kar, J. Cryst. Growth 234 (2002) 267 – 271.
[2] A. Pricilla Jayakumari, S. Dhanuskodi, S. Manivannan, Spectrochim. Acta, Part A 63 (2006) 91 – 95.
[3] D. Xue, K. Betzler, H. Hesse, D. Lammers, Solid State Commun. 114 (2000) 21 – 25.
[4] D. Xue, K. Betzler, H. Hesse, Appl. Phys. A 74 (2002) 779 – 782.
[5] G. Heller, A survey of structural types of borates and polyborates. Topics in Current Chemistry (Springer, Berlin 1986)
[6] C. Chen, B. Wu, A. Jiang, G. You, Sci. Sin. Ser. B 28 (1985) 235 – 243.
[7] C. Chen, International Conference on Laser, Xiamen, China, Nov. 1987.
[8] T. Balakrishnan, G. Bhagavannarayana, K. Ramamurthi, Spectrochim. Acta, Part A 71 (2008) 578 – 583.
[9] V. Joseph, S. Gunasekaran and V. Santhanam, Bull. Mater. Sci. 26 (2003) 383 - 386.
[10] C. Justin Raj, S. Krishnan, S. Dinakaran, S. Mary Navis Priya, R. Uthrakumar and S. Jerome Das, Cryst. Growth Des. 8 (11) (2008) 3956 - 3958.
[11] V. Chithambaram, S. Jerome Das, R. Arivudui Nambi, S. Krishnan, Optics & Laser Techno. 43 (2011) 1229 - 1232.
[12] D. Balasubramanian, R. Sankar, V. Siva Shankar, P. Murugakoothan, P. Arulmozhichelvan, R. Jayavel, Mater. Chem. Phys. 107 (2008) 57 - 60.
[13] Junye Lu, Feiyun Guo, Jianzhong Chen, J. Cryst. Growth 314 (2011) 157 – 162.

[14] M. Marezio, H.A. Plettinger, W. H. Zachariasen, Acta. Cryst 16 (1963) 975 – 980.

[15] H. Hellwig, P. Becker, S. Ahrweiler, L. Bohaty, Cryst. Res. Technol. 35 (2000) 1151 – 1161.

[16] Xingcheng Luo, Shilie Pan, Xiaoyun Fan, Jide Wang, Gang Liu, J. Cryst. Growth 311 (2009) 3517 – 3521.

[17] K. Nakamoto, Infrared and Raman spectra of Inorganic and Coordination compounds, Wiley, New York, 1978

[18] George Socrates, Infrared and Raman characteristic group frequencies, John Wiley, New York, 2001.

[19] N. Tigau, V. Ciupinaa, G. Prodana, G. I. Rusub, C. Gheorghies, E. Vasilec, J. Optoelectronics Adv. Mater. 6 (2004) 211 – 217.

[20] A. Ashour, N. El – Kadry, S. A. Mahmoud, Thin Solid Films 269 (1995) 117 – 120.

[21] R. E. Denton, R. D. Campbell, S. G. Tomlin, J. Phys. D: Appl. Phys. 5 (1972) 852.

[22] B. W. Mott, Micro Indentation Hardness Testing, Butterworths, London, 1966

[23] J. Bowman, M. Bevis, Colloid Polym. Sci. 255 (1977) 954 – 966.

[24] F. Frohlich, P. Grau, W. Grellmann, Phys. Status Solidi (A) 42 (1977) 79 – 82.

[25] E. M. Onitsch, Mikroskopie. 2 (1947) 131 - 151.

[26] H. Li, R. C. Bradt, J. Matter. Sci. 31(1996) 1065 – 1070.

[27] S. M. Dharmaprakash, P. Mohan Rao, J. Mater. Sci. Lett. 8 (1989) 1167 – 1168.

[28] K. V. Rao, A. Smakula, J. Appl. Phys. 36 (1965) 2031 – 2038.

[29] C. P. Smyth, Dielectric Behavior and structure; (McGraw – Hill; New York; 1965).

[30] N. Pattanaboonmee, P. Ramasamy, R. Yimnirun, P. Manyum, J. Cryst. Growth 314 (2011) 196 – 201.

[31] V. Ganesh, Ch. Snehalatha Reddy, Mohd. Shakir, M. A. Wahab, G. Bhagavannarayana, K. Kishan Rao, Physica B 406 (2011) 259 – 264.

[32] S. K. Kurtz, T. T. Perry, J. Appl. Phys. 39 (1968) 3798 – 3813.